A Pinatubo Climate Modeling Investigation

Conference Paper · January 1996

DOI: 10.1007/978-3-642-61173-5_20

CITATIONS
51

READS
297

31 authors, including:

Makiko Sato
Columbia University
80 PUBLICATIONS **14,148** CITATIONS
SEE PROFILE

R. Ruedy
NASA
91 PUBLICATIONS **18,362** CITATIONS
SEE PROFILE

Andrew A Lacis
NASA-GISS
225 PUBLICATIONS **22,491** CITATIONS
SEE PROFILE

Brian Cairns
NASA
253 PUBLICATIONS **6,881** CITATIONS
SEE PROFILE

A Pinatubo Climate Modeling Investigation

J. Hansen, M. Sato, R. Ruedy, A. Lacis, K. Asamoah[1], S. Borenstein[2], E. Brown[3], B. Cairns, G. Caliri, M. Campbell[4], B. Curran[3], S. de Castro[2], L. Druyan, M. Fox[3], C. Johnson[1], J. Lerner, M.P. McCormick[5], R. Miller, P. Minnis[5], A. Morrison[2], L. Pandolfo, I. Ramberran[1], F. Zaucker, M. Robinson[1], P. Russell[6], K. Shah, P. Stone[7], I. Tegen, L. Thomason[5], J. Wilder[3], H. Wilson
NASA
Goddard Institute for Space Studies
2880 Broadway
New York, NY 10025
USA

Abstract. Global cooling of the Earth's surface has been observed following the largest volcanic eruptions of the past century, although the average cooling is perhaps less than expected from simple energy balance considerations. The Mount Pinatubo eruption, with both the climate forcing and response observed better than previous volcanoes, allows a more quantitative analysis of the sensitivity of climate to a transient forcing. We describe the strategy and preliminary results of a comprehensive investigation of the Pinatubo case.

Background

Speculation about the effect of volcanoes on climate has existed at least for centuries. Benjamin Franklin, in May of 1784, wrote of a constant "dry fog" in 1783 which so dissipated the sun's rays that "when collected in the focus of a burning glass, they would scarce kindle brown paper" (Franklin, 1784; Sigurdsson, 1982). Franklin attributed the dry fog to a large Icelandic volcano, argued that the reduced solar heating was the cause of unusual cold in 1783-4, and even discussed the positive climatic feedback that may ensue from increased snow cover. Searches of more ancient literature (e.g., Stothers and Rampino, 1983; Forsyth, 1988)

---

[1] Andrew Jackson High School, 207-01 116th Avenue, Cambria Heights, NY 11411
[2] York College, 94-20 Guy R. Brewer Blvd., Jamaica, NY 11451
[3] Bronx High School of Science, 75 West 205th St., Bronx, N.Y. 10468
[4] City College of New York, 135th Street and Convent Avenue, NY 10031
[5] NASA Langley Research Center, Hampton, VA 23665
[6] NASA Ames Research Center, Moffett Field, CA 94035
[7] Massachusetts Institute of Technology, Center for Meteorology, Cambridge, MA 02139

NATO ASI Series, Vol. I 42
The Mount Pinatubo Eruption
Effects on the Atmosphere and Climate
Edited by Giorgio Fiocco, Daniele Fuà and Guido Visconti

have uncovered many references to impacts of volcanoes on sunlight at the Earth's surface and many references to observed climate anomalies, but no attribution of climate anomalies to volcanoes.

The largest aerosol amount during the past two centuries was apparently that produced by the Tambora eruption in 1815, which caused an atmospheric opacity estimated to be several times greater than either Krakatau in 1883 or Pinatubo in 1991 (Stothers, 1984). Tambora was followed, in 1816, by the "year without a summer" (Stommel and Stommel, 1979, 1983) with abnormal cold in the Eastern United States and Europe. A clockmaker in Plymouth Connecticut wrote "On the 10th of June, my wife brought in some clothes that had been spread on the ground the night before, which were frozen stiff as in winter. On the 4th of July I saw several men pitching quoits in the middle of the day with thick overcoats on, and the sun shining bright at the time" (Stommel and Stommel, 1979). Of more practical importance, there were killing freezes in the Northeast United States on June 10, July 9 and August 21, 1816. That same summer excessively damp, cool weather in Europe forced Lord Byron and Mary and Percy Shelley to remain indoors, where they competed in writings fitting the climate, Byron producing his poem "Darkness" (original handscript reproduced as frontispiece of Harington, 1992) and Mary Shelley writing a short story later expanded to the novel "Frankenstein". There was widespread crop failure in Europe and India, and it has even been speculated that the resulting Indian famine played a role in the widespread outbreak of cholera (Stommel and Stommel, 1979).

Despite this evidence for large regional climate anomalies, when worldwide evidence for climate change after Tambora was examined in detail (Wilson, 1992) the results were found to be mixed, with some regions showing little temperature change or even warming. This may only indicate that global cooling due to the volcano was less than regional climate variability. Instrumental temperature data, based on about 50 stations in the Northern Hemisphere, suggest a mean cooling of about 0.5°C, not much more than the year-to-year variability for those stations (Stothers, 1984).

Volcanic cooling may be easier to detect in the period when global temperature data is available, because unforced climate variability is much smaller on the global scale than on the

regional scale. During the time of nearly global instrumental temperatures, i.e., since about 1880, the volcanoes producing the greatest aerosol optical depth are Krakatau and Pinatubo (Sato et al., 1993). Both volcanoes were tropical and their aerosols were probably spread globally, although that is an assumption for Krakatau because of the absence of Southern Hemisphere observations. Three other low latitude volcanoes, Santa Maria in 1902, Agung in 1963 and El Chichon in 1982, produced global mean aerosol optical depths at least half as large as for Pinatubo (Sato et al., 1993). The estimated global mean optical depth at visible wavelengths for Santa Maria, Agung and El Chichon reached maximum values close to 0.1, while the maximum values for Krakatau and Pinatubo were probably about 0.15 (Sato et al., 1993).

The mean global temperature change after these five volcanoes, Fig. 1 (a), shows evidence of cooling. The data is presented in several different ways: the upper curve is the estimated mean global temperature anomaly, the second curve is for the Northern Hemisphere, and the third curve is for the Northern Hemisphere after the temporal scale has been seasonally synchronized (t = 0 being July 1 of the year of eruption). Because the global averages of both aerosol optical depth and surface air temperature are especially uncertain in the Krakatau era, we have also presented, in Fig.1 (b), results with Krakatau excluded.

The temperature zero point in Fig. 1 is defined as the mean for the 12 months preceding the eruption. If we instead defined the zero point as the temperature at the time of eruption, or as the mean temperature of the preceding five years, the magnitude of the cooling after the eruption would be less, but if we used the two years before the eruption to define the zero point the apparent cooling would be somewhat greater. Thus the magnitude of the cooling is inherently uncertain by about 0.05-0.1°C as a result of climate variability ("noise") and the small number of cases available for averaging.

Another source of uncertainty is the incomplete spatial coverage of the temperature measurements. The meteorological stations used as the basis for global temperature estimates of Hansen and Lebedeff (1987) result in a land bias, although the weighting of coastal and island stations reduces that bias. When more complete open ocean data is combined with the land data the global cooling is reduced somewhat (IPCC, 1992), as expected because of the

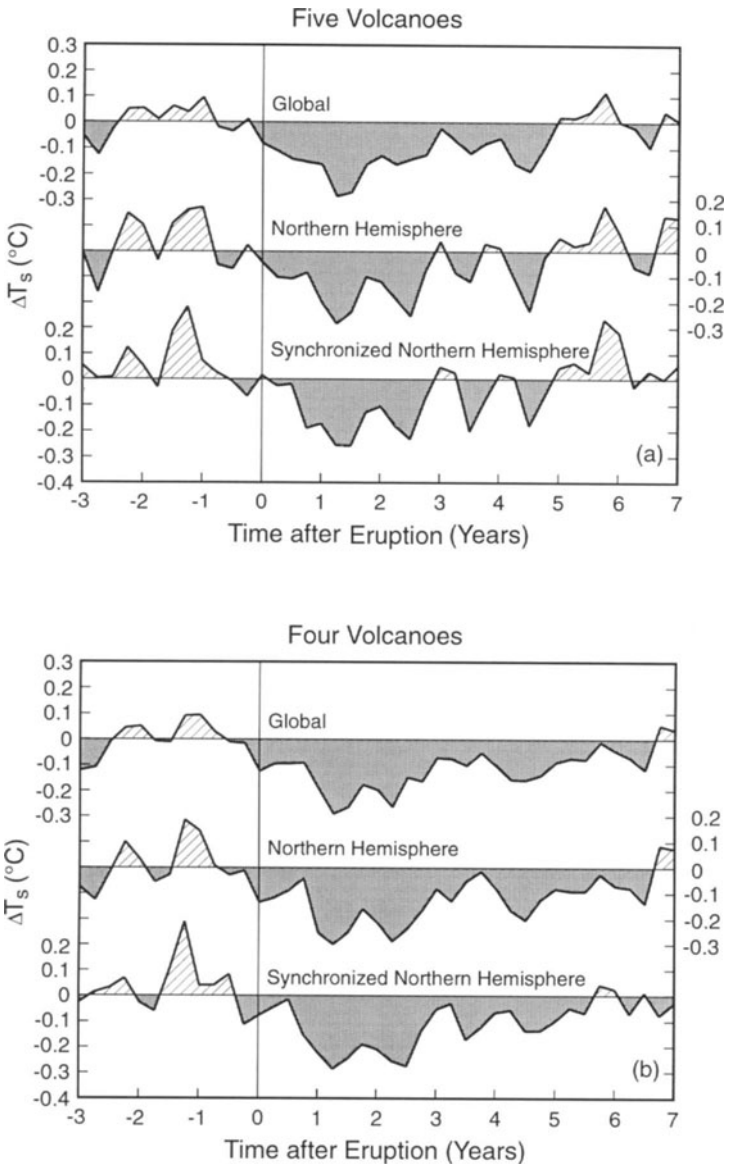

Figure 1. (a) Mean surface air temperature near the time of eruption for the five volcanoes producing the greatest optical depths in the past century: global, Northern Hemisphere, and Northern Hemisphere seasonally synchronized. (b) Results when Krakatau is excluded from the average. Temperature estimates are based on an update of Hansen and Lebedeff (1987). All curves are three month means. In (a) and (b) Pinatubo contributes only through 3.5 years after its eruption.

ocean's large thermal inertia. But the temperature series based on land plus ship data are also imperfect, underweighting high latitude and sea ice regions where climate sensitivity is highest. Therefore we believe that the temperature anomalies of Fig. 1 are close to the best estimate available.

Bearing in mind the above sources of uncertainty, we conclude that the average cooling after these large eruptions reached a maximum of about a quarter of a degree, 0.25±0.1°C, with most substantial cooling in the period 1-3 years after the eruption. Fig. 1 suggests that some cooling effect may have lasted as much as 6-7 years, a result somewhat different from previous analyses of the composite response to volcanoes (Mitchell, 1961; Mass and Schneider, 1978; Self and Rampino, 1988). Although the negative temperature anomaly in years 4-7 after the eruption is small, it seems noteworthy because most of these volcanoes occurred during a period of long-term warming.

The observed maximum surface cooling after large volcanoes seems to be somewhat less than has been suggested by climate model calculations (Robock, 1983). Climate models which incorporate the effects of continents and oceans and treat the ocean heat capacity in ways neglecting dynamical feedbacks typically yield a maximum global cooling of about 0.5°C, for volcanoes with maximum aerosol optical depth 0.1-0.15. The broad range of such models includes energy balance models (Schneider and Mass, 1975; Robock, 1984, Gilliland and Schneider, 1984), 1-D radiative-convective models (Hansen et al., 1978), 2-D dynamic models (MacCracken and Luther, 1984), and simple GCMs (Hunt, 1977; Hansen et al., 1992). It is noteworthy that none of these models realistically portrays the interactions of surface climate with either ocean dynamics or stratospheric dynamics.

A discrepancy between observed and calculated climate response could result from either inaccurate specification of the climate forcing or inaccurate sensitivity of the climate models. We examine the accuracy of the climate forcing in Section 7. The data available for Pinatubo provides the first opportunity to test fundamental questions about the magnitude of volcanic aerosol climate forcing. Because it is possible to define accurately the forcing due to Pinatubo, that means it will also be possible to use Pinatubo as a test of climate sensitivity to a given forcing.

Given an accurate aerosol climate forcing, if there is a discrepancy between climate model response and observed climate change, the candidates for explaining it include:

1. Underestimate of the effective ocean heat capacity, including the possibility that volcanoes may induce or enhance El Ninos (Handler, 1986; Rind et al., 1992) or affect stratosphere-troposphere interactions so as to increase the flow of marine air over the continents in winter (Robock and Mao, 1992; Kodera, 1993; Graf et al., 1993, 1994; Kodera and Yamazaki, 1994).

2. Inaccuracy of the assumed net climate forcing, including the possibility that volcanoes may induce a climate forcing, for example, by seeding cirrus clouds (Jensen and Toon, 1992; Sassen et al., 1995; Wang et al., 1995).

3. Inaccuracy of the (equilibrium) climate sensitivity of the models. This third possibility is an unlikely explanation, because paleoclimate evidence strongly supports the magnitude of climate sensitivity in the models and, furthermore, the short-term response to volcanic aerosol forcing depends only weakly on equilibrium climate sensitivity (Hansen et al., 1993).

Overall, we conclude that the connection of volcanoes and climate change has remained substantially anecdotal and much less quantitative than desired (Self and Rampino, 1988; Robock, 1991), in part because of the difficulty of identifying volcanic effects in the presence of large natural climate variability. However, Pinatubo produced probably the largest climate forcing of any volcano in the twentieth century, its climate forcing can certainly be defined most precisely, and it has the most accurately observed climate response. Thus it provides an excellent opportunity to test our understanding of the climate system's response to a large transient global climate forcing. Of course, there are limitations inherent in analysis of a single eruption, especially an eruption occurring at a time of other significant forcings such as changing greenhouse gases, but these complications can be at least partially overcome with an appropriate strategy of investigation.

Early Pinatubo Prediction

It was obvious soon after the 1991 eruption of Mount Pinatubo that the aerosol amount was unusually large. On the basis of data presented at an interagency meeting on 11 September 1991 in Washington D.C., Hansen et al. (1992) estimated that the Pinatubo forcing would be about 1.7 times greater than for the El Chichon eruption of 1982. Hansen et al. (1992) thus carried out climate simulations with a climate model previously used for predictions of greenhouse climate effects (Hansen et al., 1988). The objective was to test the model and our understanding of the climate system response to a large radiative forcing.

There are merits in carrying out this test with a model previously used for greenhouse studies. But it must be recognized that this model has deficiencies which may especially limit its ability to simulate accurately the response to this particular forcing, which is a short-term transient forcing with a substantial stratospheric component. The physics in the model is of early 1980s vintage, as described by Hansen et al. (1983). The horizontal resolution, 8 by 10 degrees, limits the realism of atmospheric dynamics. The vertical resolution of the nine model layers, with only 1-2 layers in the stratosphere, is not expected to provide realistic dynamical interactions between the troposphere and stratosphere. The fact that the model uses specified ocean heat transports with fixed mixed layer depth and diffusion into the deep ocean (Hansen et al., 1984) eliminates impact of the aerosols on El Ninos and on the depth of ocean mixing. On the other hand, the model has a sophisticated treatment of atmospheric radiation, and there is merit in first studying the radiative energy balance, with dynamics treated in simple ways, and subsequently examining the implications of more realistic dynamics.

Predicted and observed temperatures near the time of the Pinatubo eruption are shown in Fig. 2. The left half of the figure is an update of a figure presented at a Chapman conference on Pinatubo in early 1992 and published in a special report of the American Geophysical Union (AGU, 1992). The observations are ones that were readily available to us before that conference. For the sake of consistency, in subsequent updates of the model-data comparisons (e.g., Hansen et al., 1993) we have used the same data sources, although more comprehensive observations are now available. The modeled temperature is the mean of the two runs, P1 and P2, of Hansen et al. (1992). There is good semi-quantitative agreement between the model

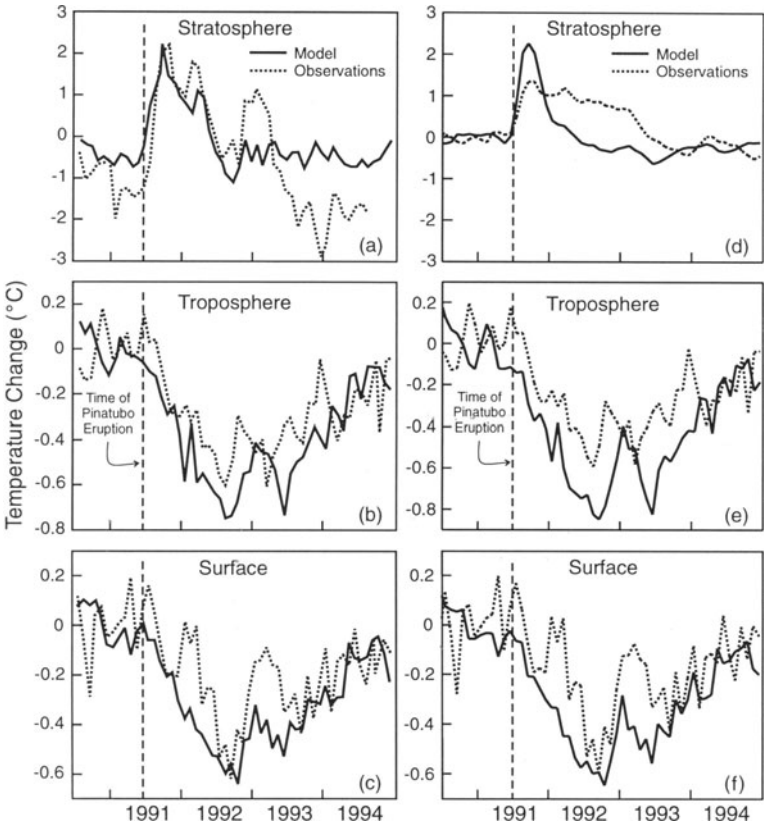

Figure 2. Left side: observed and modeled temperature change near the time of Pinatubo eruption, an update of Fig. 11 of AGU (1992) and Fig. 24 of Hansen et al. (1993). Stratospheric observations are 30 mb zonal mean temperature at 10°S provided by M. Gelman based on TOVS (Tiros Operational Vertical Sounder) measurements referenced to the 1978-1992 mean (Gelman, 1991); model results are 10-70 mb layer at 8-16°S, also referenced to 1978-1992. Tropospheric observations are MSU channel 2R (Spencer et al., 1991); model results are the mean temperature of layers 1-4 (surface to 550 mb) in runs P1 and P2 of Hansen et al. (1992). Surface air observations are derived from meteorological station data (Hansen and Lebedeff, 1987). The troposphere and surface data are referenced to the 12 months preceding the Pinatubo eruption. Right side: similar to left except all three levels are referenced to the 12 months before the month of the Pinatubo eruption, stratospheric observations are global, vertical weighting functions are applied to the model stratospheric and tropospheric data (Table 1), the model surface air temperatures are averaged over only the region with observational data, and the seasonal cycle is removed from the model by differencing with the previous 10 model years rather than by subtracting the control run. Stratospheric observations are MSU channel 4 (Spencer and Christy, 1993). Tropospheric observations are MSU channel 2R. Surface observations are an update of Hansen and Lebedeff (1987).

and observations, with stratospheric warming of a few degrees and lower tropospheric and surface cooling of about half a degree, but the modeled stratospheric warming is too short-lived and the modeled tropospheric and surface coolings are somewhat greater than observed.

In the right half of Fig. 2 for the sake of uniformity we have defined the temperature zero point at all three atmospheric levels as the mean anomaly for the 12 months preceding the month of eruption, we have weighted the model results to match observing system weightings, and for the stratosphere we have substituted more global observations. Also we remove the seasonal cycle from model monthly anomalies in a way similar to that used for the observations, by subtracting the mean monthly temperatures in the decade preceding the eruption, rather than by subtracting a control run. This alternative way of removing the seasonal cycle alters the appearance of peaks and valleys in the curves slightly, but does not change the overall comparison.

The more global comparison in Fig. 2d shows clearly the difference between the modeled and observed stratospheric response, with the modeled stratospheric temperature returning to normal much more quickly than in the real world. The reason for this can be traced to the assumed time history of the aerosol size distribution, as we show in Section 7 below. Specifically, the simulation of Hansen et al. (1992) employed the aerosol size distribution history measured at one locale by Hofmann and Rosen (1983) after El Chichon, with the aerosol size being more than 1 micron shortly after the eruption and decreasing to about a half micron by about six months after the eruption. In reality the Pinatubo aerosols grew in size for about a year after the eruption, and the size distribution had sufficient large particles to produce a substantial infrared optical depth for more than a year (Section 7).

Observations of the lower troposphere (Fig. 2b,e) show obvious cooling after the eruption, as pointed out previously by Dutton and Christy (1992). The model cooling is somewhat greater in Fig. 2e than in Fig. 2b, because in Fig. 2e the calculated tropospheric temperature change has been multiplied by the Microwave Sounding Unit (MSU) channel 2R vertical weighting function (Table 1). On the average the observed cooling is somewhat less than in the model.

Table 1. Vertical weighting profiles used for application to GCM temperatures to obtain comparisons with MSU data, based on midlatitude standard atmosphere radiative computations (Shah and Rind, 1995).

layer	pressure (mb)	land		snow		sea ice		ocean		
		Ch 2	Ch2R	Ch 2	Ch 2R	Ch 2	Ch 2R	Ch 2	Ch 2R	Ch 4
9	10-70	.046	-.010	.046	-.010	.046	-.010	.046	-.010	.584
8	70-150	.074	-.007	.075	-.007	.075	-.007	.075	-.006	.361
7	150-255	.117	.015	.117	.016	.118	.016	.119	.018	.053
6	255-390	.167	.082	.168	.084	.169	.086	.170	.088	.002
5	390-550	.185	.179	.187	.183	.188	.187	.191	.191	.000
4	550-720	.156	.226	.159	.232	.162	.239	.165	.247	.000
3	720-854	.091	.164	.094	.171	.097	.179	.102	.190	.000
2	854-934	.042	.083	.044	.090	.047	.096	.051	.105	.000
1	934-984	.022	.046	.024	.051	.027	.056	.030	.064	.000
surface		.101	.222	.086	.190	.071	.158	.051	.113	.000

The comparison of surface air temperatures of the model and observations (Fig. 2c) can be made more consistent either by adding measurements of surface air temperature over the ocean to the observations or by sampling the model at the locations of the meteorological stations. Results of the latter approach are illustrated in Fig. 2f. Results of the former approach are illustrated in Fig. 1.6 of the Sixth Annual NOAA Climate Assessment (NOAA, 1995), which was obtained by combining nighttime marine surface air temperatures with the meteorological station data. The resulting global temperature curve is qualitatively very similar to our observational curve in Fig. 2c, with maximum cooling of 0.5°C in Sep-Oct-Nov of 1992, and an overall temperature curve similar to that from the model with the two major exceptions of Jan-Feb-Mar in both 1992 and 1993. These Northern Hemisphere winters were both about 0.4°C warmer than the model results, with the warmth occurring over Asia and North America. Although this is consistent with the Kodera and Yamazaki (1994) suggestion for stratospheric influence, it is also consistent with El Nino influence on Pacific North American

(PNA) temperature patterns, and, furthermore, the unforced variability of surface air temperature is largest in Northern Hemisphere winters, as we illustrate in Section 5 below.

This cursory examination suggests that the climate response after Pinatubo is probably consistent with the typical response observed after previous large volcanoes, i.e., there is evidence of surface cooling but a suggestion that the global average magnitude of the cooling may be somewhat smaller than simple energy balance considerations would suggest. In the case of Pinatubo we believe that it will be possible to come to a more definitive conclusion.

However, satisfactory analysis of this natural Pinatubo climate experiment requires a comprehensive strategy of investigation. It requires first of all a capability for more realistic climate modeling than that used in the above study, but also a strategic sequence of numerical simulations. In addition we must define and verify the Pinatubo aerosol climate forcing with greater accuracy than was possible in 1992, as we discuss in Section 7.

Strategy of Investigation

Our objective is to use available information on Pinatubo aerosols and other climate forcings of the past decade, together with data on observed climate change, to extract knowledge about climate sensitivity. This objective demands that our tools for simulating climate be capable of realistically representing climate on regional scales. This is required even to analyze the global mean response, because the dynamical pattern of anomalies affects global mean quantities. Furthermore, the ultimate goals of these climate studies must include the impact on society, and that is a function of the regional pattern of climate change.

Thus our quantitative studies are dependent upon having a climate model with sufficient realism and spatial resolution to adequately represent continental and subcontinental scale climate characteristics. In view of the large interannual variability of climate on such scales, even without any forcings, it is also clear that we must plan on making multiple numerical climate experiments and assessing the frequencies or probabilities of climate anomalies.

Examples of climate anomalies of interest are shown in Fig. 3a. Northern Hemisphere anomalies after Pinatubo include very cool continents in the summer of 1992, a cool summer in 1993 with record floods in the midwest United States, a warm 1991-2 winter in North America and Asia, and extreme cold in the eastern United States in winter 1993-4.

For comparison with the surface anomalies of Fig. 3a we show the corresponding MSU channel 2 (Spencer et al., 1991) anomalies in Fig. 3b. MSU channel 2 principally records tropospheric temperature, but about 12 percent of its weighting function is in the stratosphere (Table 1). The MSU channel 2 anomalies have a high degree of spatial correlation with the surface anomalies, but tend to be smaller in magnitude. One advantage of the MSU data is its nearly global coverage.

Perhaps our greatest challenge will be to characterize adequately the climate models employed. In particular, our study must be designed to demonstrate that the principal conclusions about the climate system are not sensitive to model deficiencies, which will always exist to some degree.

In our modeling studies we begin with the most current version of the GISS global climate model, in which many of the physical processes and numerical schemes of model II (Hansen et al., 1983) have been replaced by more realistic alternatives. We use a horizontal atmospheric resolution of 4 by 5 degrees, which seems potentially capable of resolving the major climate anomalies in Fig. 3 but still allows us to perform ensembles of experiments as required to calculate the statistical significance of results. Determination of the capabilities of this model is a key part of our strategy of investigation, which we summarize here.

Model characterization. First, the atmospheric model is characterized in the standard way, by making a run of at least several years with specified climatological sea surface temperatures and comparing the simulated climate with available observations. Second, the model is used for a transient simulation of the extended AMIP (Atmospheric Model Intercomparison Project) period, 1979-1993, using observed transient sea surface temperatures, with results submitted to the AMIP project (Gates, 1992); this allows characterization of the model's ability to respond to transient forcings such as El Nino sea surface temperature anomalies. Third, broad

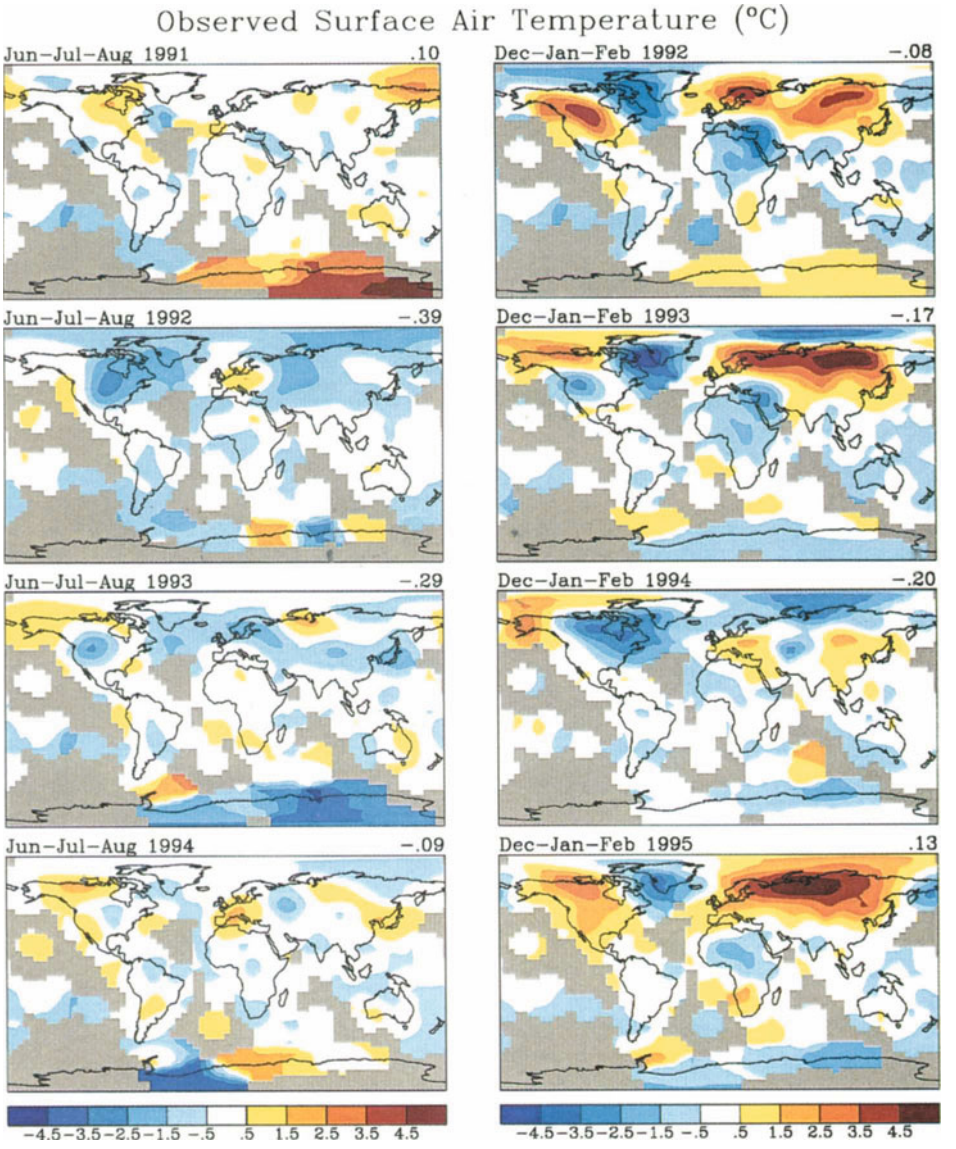

Figure 3a. Observed seasonal surface air temperature anomalies of the past four years. Data are an update of Hansen and Lebedeff (1987). Local monthly anomalies are computed relative to 1951-1980 monthly means and then adjusted by a single additive constant so that the 12 month mean from June 1990 through May 1991 is zero.

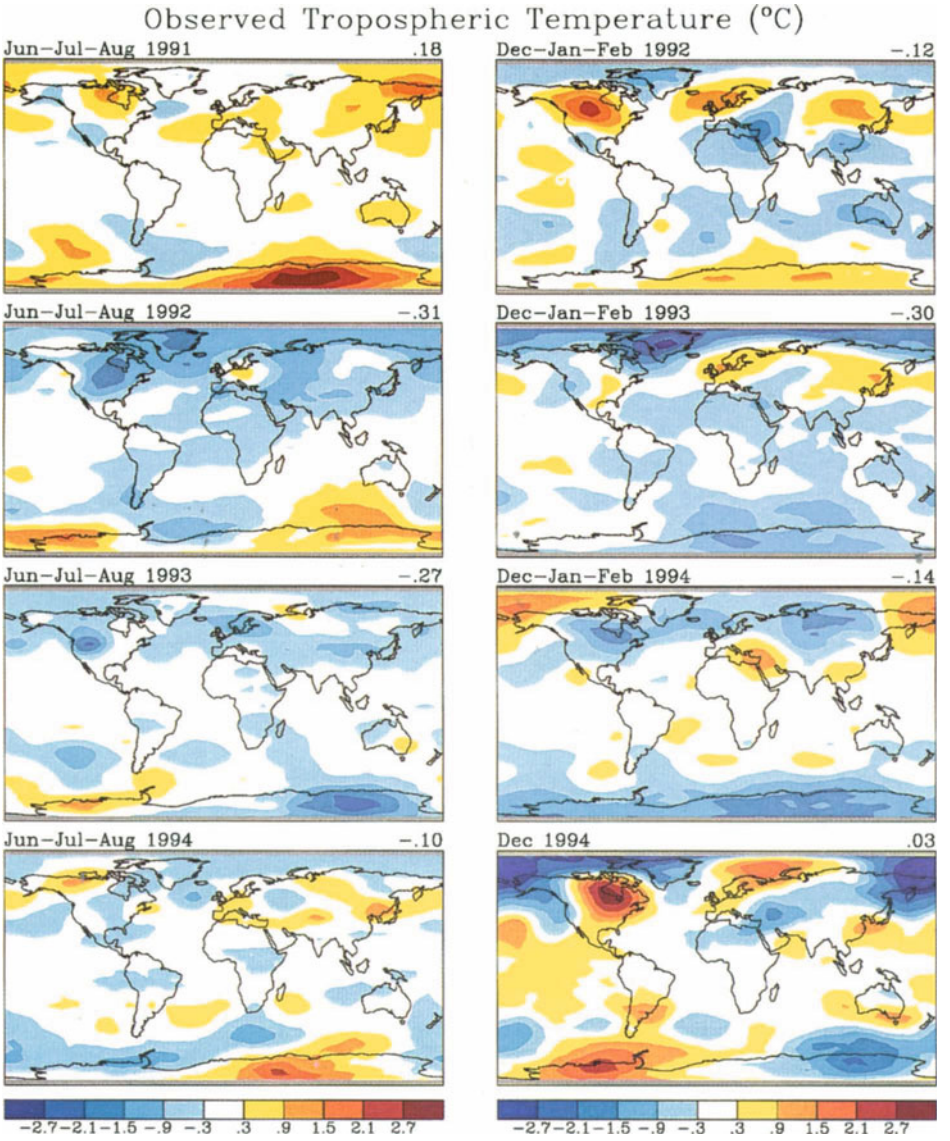

Figure 3b. Observed seasonal tropospheric temperature anomalies of the past four years. Data are MSU channel 2 (Spencer et al., 1991). Local monthly anomalies are computed relative to 1979-1993 monthly means and then adjusted by a single additive constant so that the 12 month mean from June 1990 through May 1991 is zero.

use of the identical model by GISS scientists and outside collaborators is encouraged, because it is only after a model has been exercised in many ways that its capabilities can be characterized well. Model diagnostics from key control runs and experiments will be made available over the internet system.

Radiative forcing experiments. Each radiative forcing, e.g., Pinatubo aerosols, ozone change, and homogeneously mixed greenhouse gases, will be added sequentially, with the model run five times over the period 1979-1990 and 25 times over 1991-1995. The number of runs is intended to be sufficient to provide an indication of the significance of global trends over the 1979-1995 period and the significance of regional anomalies subsequent to the Pinatubo eruption.

Ocean component. The experiments will be run with the ocean treated in three different ways: specified sea surface temperature (SST), calculated SST with specified ocean heat transport (Q-flux), and calculated SST with at least one dynamically interactive ocean. This set of experiments provides a powerful basis for analyzing the role of the ocean in observed climate change, helping us to study the roles of energy fluxes at horizontal interfaces, atmospheric dynamics and ocean dynamics.

Model improvements. A version of the model (SI94) was "frozen" for the 1994 GISS Summer Institute on Climate and Planets for the first set of experiments. Model development is proceeding in parallel with the experiments, and it is planned to freeze improved versions of the model again in later years, and to repeat experiments with the new models using the same forcings employed in SI94. Model climatologies will always have substantial deficiencies compared to the real world, but if it can be shown that the inferences from the model remain unchanged as the model climatology becomes more realistic, that will help solidify the conclusions.

Educational component. Our model testing, experiments, and analyses are being carried out with the involvement of students and educators from New York City high schools and colleges. One of our objectives is to aide in the teaching of how science works by developing a research component for school curricula. We hope that ultimately this will improve

communication with the public about the nature of scientific research, and improve understanding of the difficult subject of global climate change. We expect this collaboration to improve the quality of our research product via the contributions of the new researchers, and also via the efforts that will be needed to describe the research process for such a broad community.

The tasks presently defined for the students in the Pinatubo project are, for a given climate parameter (temperature, precipitation, winds, radiation balance), to: (1) map and compare the model climatology and observations, (2) map and compare the interannual variability of their parameter in the model and observations, (3) map and describe the anomalies of their parameter during the period following Pinatubo, (4) map and analyze the simulated climate anomalies for a succession of climate forcing experiments. Each student studies a parameter for one season, either December-January-February (DJF) or June-July-August (JJA), with results compared among students and attempts made to understand the relationships among different parameters.

In the following two sections we show results from the first two tasks. An example of results from the third task was shown in Fig. 3. The simulations required for the fourth task are now underway.

Model vs. Climatology

During the past decade new versions have been developed for most of the components of GISS model II (Hansen et al., 1983). Objectives of the model development are to both improve the realism of the model and increase the range of problems to which the model can be usefully applied. We summarize here changes included in the SI94 version of the model. It is expected that the model tests and applications in the Pinatubo project will lead to a significantly improved model.

The current model includes a prognostic cloud water parameterization which calculates cloud optical properties (Del Genio et al., 1995) and an improved parameterization of moist convection including the effects of convective downdrafts and mesoscale cirrus anvils (Del

Genio and Yao, 1993). A new planetary boundary layer parameterization employs a finite modified Ekman layer with parameterizations for drag and mixing coefficients based on similarity theory (Hartke and Rind, 1995). The land surface parameterizations now include explicit modeling of the vegetation canopy and modeling of the soil water with underground runoff (Rosenzweig and Abramopoulos, 1995).

Horizontal resolution is 4 by 5 degrees, but the vertical resolution has the identical nine layers of model II. Fourth order numerical differencing (Abramopoulos, 1991) is used for the momentum equation, a quadratic upstream scheme (similar to that of Prather, 1986) is used for heat and moisture, and a weak Shapiro filter is applied to the horizontal winds to remove high wave number noise.

As in model II, a large number of vegetation types are represented by appropriate fractions of a small suite of vegetation types (Matthews, 1984), but several changes are made to improve the realism of the albedo and to incorporate cultivated land. The single albedo value for desert is replaced with ISCCP albedo measurements (Rossow and Zhang, 1995) over bare soil areas, thus generally increasing the reflectance in Saharan and Arabian regions and decreasing it in arid regions of Australia, Asia, North America and southern Africa. The impact of agriculture is included using a data set for cultivation intensity (Matthews, 1983) which defines the cultivated fraction of cells at 1-degree resolution. Cultivated land is thus a separate category in the model, with, at present, its characteristics being identical to those of grassland. The ocean albedo is modified to account for foam at high wind speed and subsurface scattering (H. Gordon, priv. comm.).

Run 1a of model SI94 (Table 2) is the climatological control run, with specified seasonally varying sea surface temperature (SST) based on a 15 year (1979-1993) average of Reynolds (1988) and Reynolds and Marsico (1993) blended (ship and satellite) data set. This is the SST and sea ice data set used for the AMIP project (Gates, 1992).

The surface air temperatures produced by run 1a for DJF and JJA are compared with observations in Fig. 4. Although the model succeeds in generating climate patterns similar to the observations, the difference map reveals significant model errors, the largest being

Table 2. GISS SI94 GCM control runs.

Run #	Years /Date	No. of[1] Runs	Run Description
1	25	1	Climatological SST with seasonal cycle, 1980 gas amounts. Run 1a uses 1979-93 means of Reynolds and Marsico SST and sea ice; run 1b uses their 1982-87 mean SST and sea ice[2].
2	1979-93	5/25	Run 1a with observed time-varying SST (mean sea ice)
3	1979-93	5/25	Run 1a with observed time-varying SST and sea ice
4	50	1	Run 1b with Q-flux mixed-layer ocean
4*	50	1	Run 4 with 2*CO2
5	20+	1	Run 1b with Q-flux mixed-layer + diffusive deep ocean
6		1	Run 1b with Russell's ocean model (G. Russell et al., 1995)
7		1	Run 1b with Fung's ocean model (Jiang and Fung, 1994; Miller and Jiang, 1995)

[1] Under "# of runs" 5/25 means 5 runs for the 12-year period 1979-1990 and 25 runs for the period beginning January 1, 1991.

[2] Run 1b also is modified slightly so that the sea ice albedo is reduced when the temperature is near melting, and the solar irradiance is reduced slightly (about 1%) so that the planet is exactly in radiation balance. The climatologies of runs 1a and 1b differ very little.

excess warmth over Canada in winter. Elsewhere the largest errors in surface air temperature are located in and around regions of high topography. The surface wind errors, shown by arrows in Fig. 4c, are consistent with the temperature errors, but are not sufficient to identify the ultimate source of the problems.

Tropospheric temperatures are shown in Fig. 5. Some of the problems in the surface temperature simulation are absent or reduced, suggesting that these problems may involve primarily surface and boundary layer aspects of the simulations. Even the reduced error in regions of topography may originate largely at the surface, as MSU channel 2 receives 5-10%

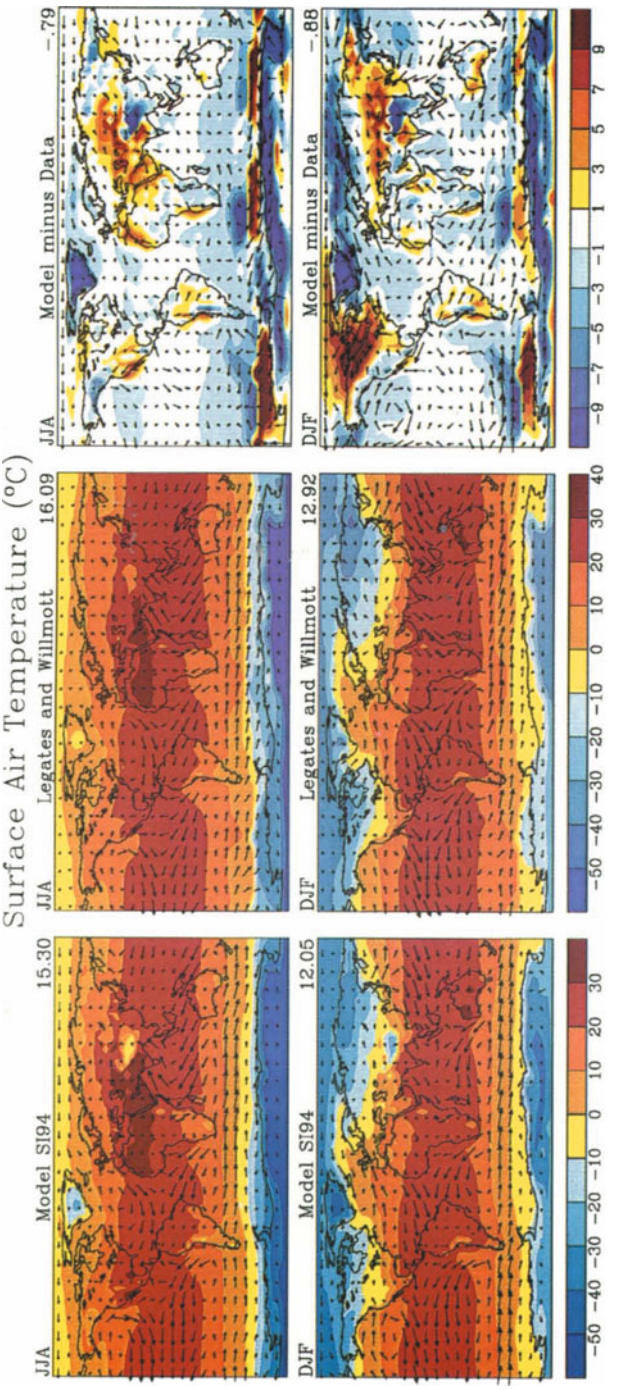

Figure 4. Modeled and observed surface air temperature for JJA (above) and DJF (below). Model is run 1a of GISS SI94 model, which has specified mean 1979-93 SST (Table 2). Observations are climatology of Legates and Willmott (1990a). Length of wind arrows is proportional to surface wind speed, the observations being based on the climatology of Oort (1983).

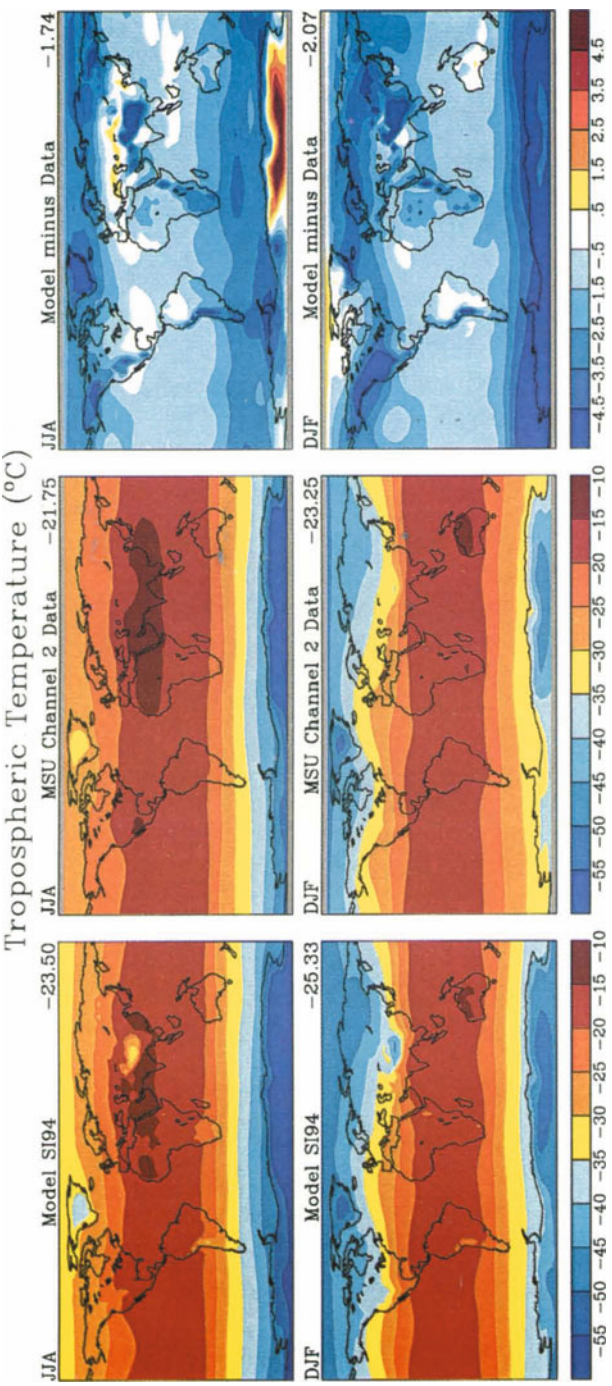

Figure 5. Modeled and observed tropospheric temperature for JJA (above) and DJF (below). Model is run 1a of GISS SI94 model. Observations are MSU channel 2 (Spencer et al., 1991).

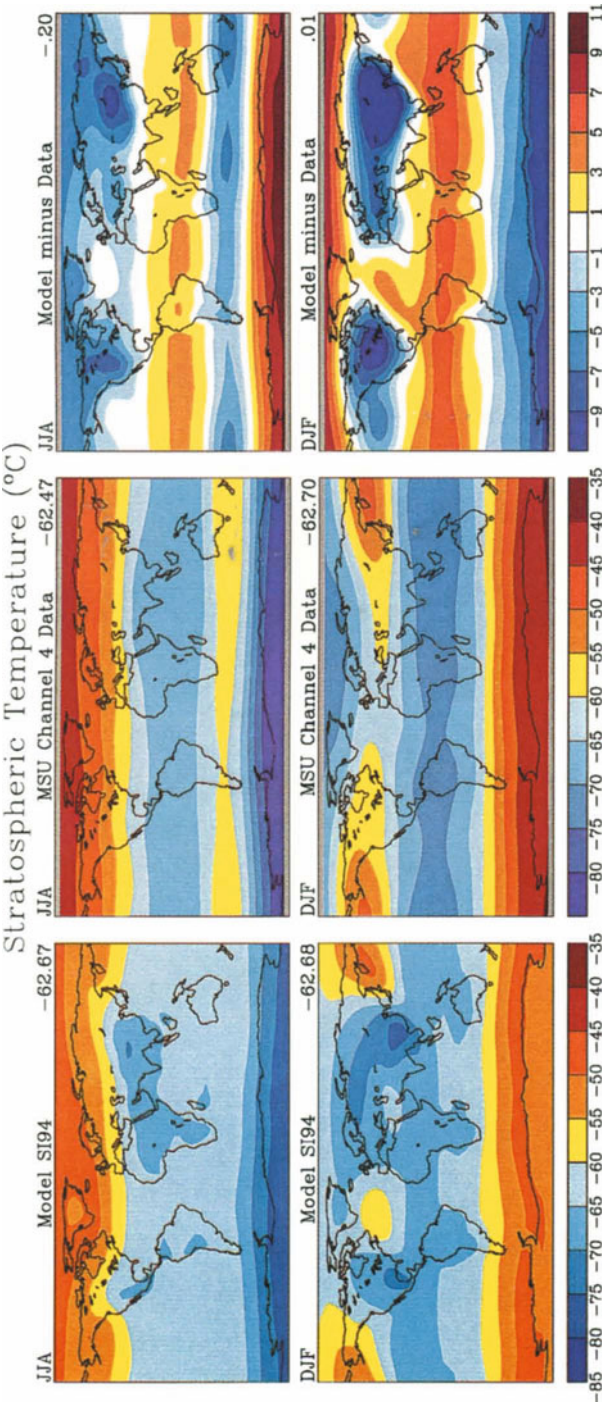

Figure 6. Modeled and observed stratospheric temperature for JJA (above) and DJF (below). Model is run 1a of GISS SI94 model. Observations are MSU channel 4 (Spencer and Christy, 1993).

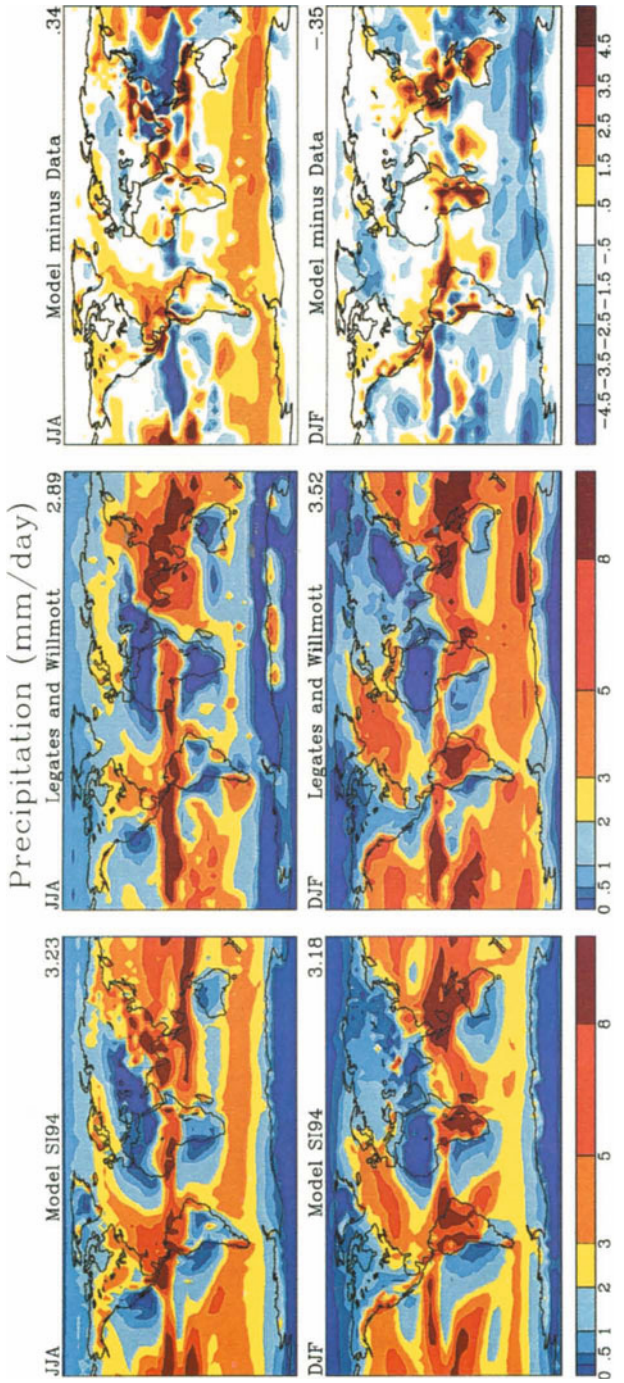

Figure 7. Modeled and observed precipitation for JJA (above) and DJF (below). Model is run 1a of GISS SI94 model. Observations are climatology of Legates and Willmott (1990b).

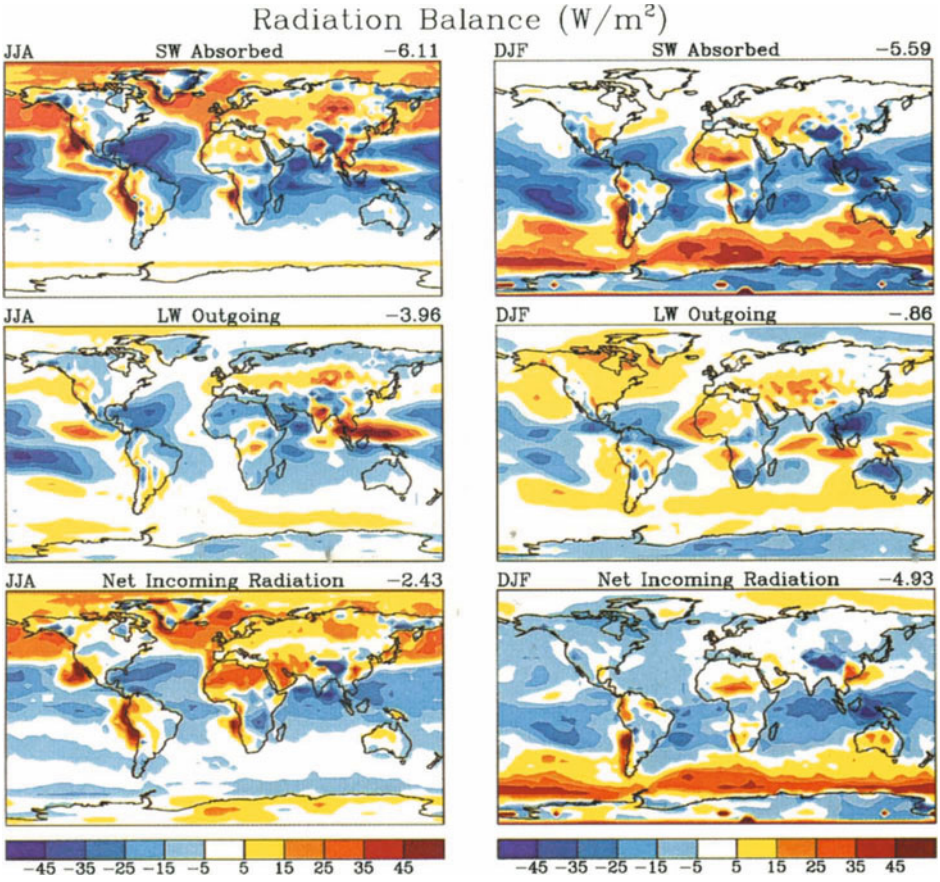

Figure 8. Difference between modeled and observed absorbed solar radiation, emitted thermal radiation, and net radiation balance, for JJA (left) and DJF (right). Model is run 1a of GISS SI94 model. ERBE observations (Barkstrom et al., 1989) are 1985-89 mean.

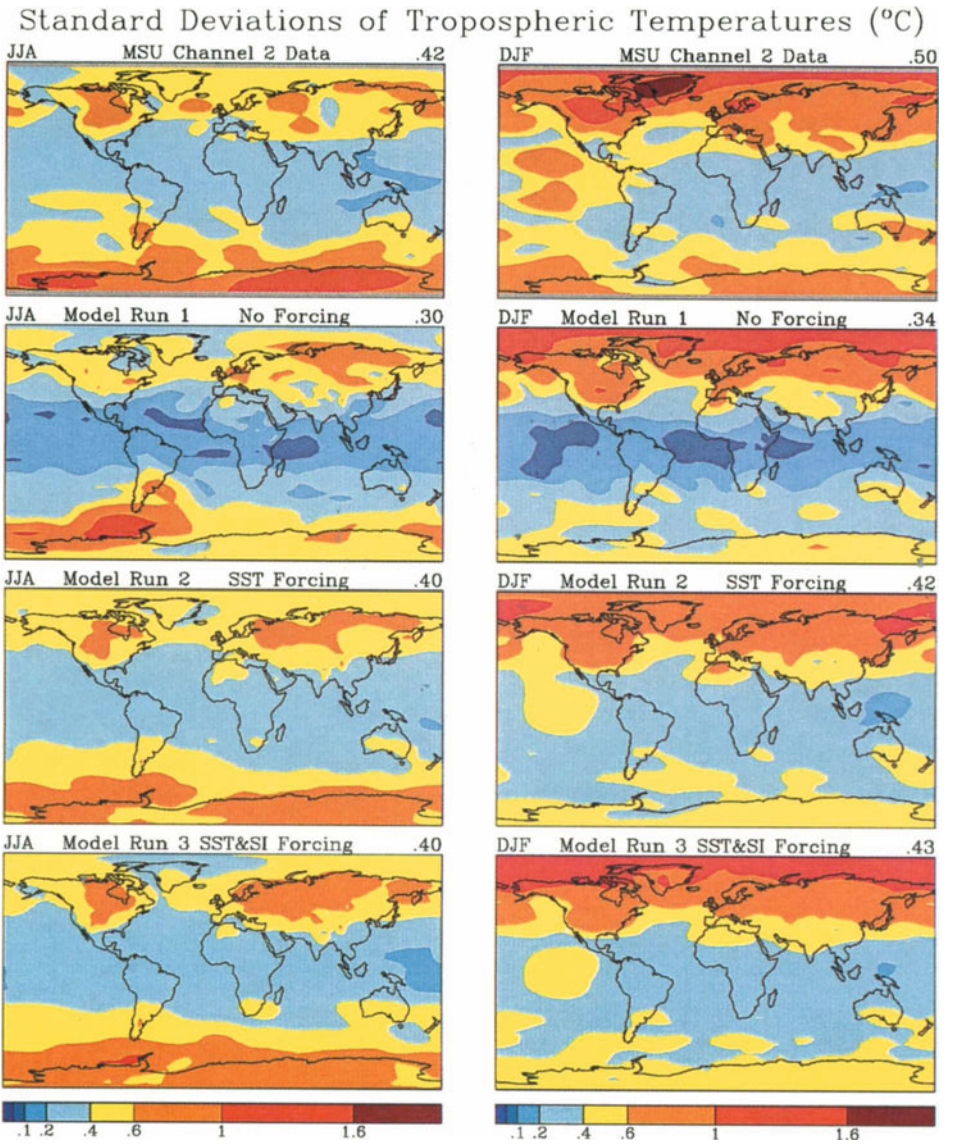

Figure 9. Standard deviation of tropospheric temperature in observations (MSU channel 2) and in the GISS SI94 model. Model run 1 has no forcing, i.e., climatological sea surface temperature and sea ice (SST and sea ice), run 2 has interannually varying SST, and run 3 has interannually varying SST and sea ice. In the last case, run 3, the sea ice variability is unrealistically large. The standard deviations of seasonal means are computed for 15 seasons from 1979-93, except run 1 which had 25 seasons. Runs 2 and 3 were repeated 5 times, with the standard deviations computed for each of the five runs and then averaged.

of its signal from the surface (Table 1). The troposphere is generally too cool in the model, especially at high latitudes, implying that the tropospheric lapse rate is too large.

Stratospheric temperatures are shown in Fig. 6. In this case there are qualitative and quantitative errors in the simulated climate. The model is too cold at high latitudes in summer, while it is too warm in the tropics and at the winter pole. The winter long-wave patterns are not captured by the model, with the model much too cold over North America and Asia. Such errors in the stratosphere are not surprising, as the model has only 1-2 stratospheric layers, has a rigid model lid located at about 30 km altitude, and has artificial drag in the top layer to prevent excessive zonal winds. Aspects of these errors persist in models with higher vertical resolution and may be related to unresolved gravity wave effects (Rind et al., 1988).

The precipitation is shown in Fig. 7. The precipitation distribution in model SI94 is generally more realistic than in model II, which can be traced to the new boundary layer and moist convection parameterizations (Marengo and Druyan, 1994). The greatest disagreements with observations are in the equatorial rainbelts. In the Western Pacific in JJA the intertropical convergence zone (ITCZ) is about 15 degrees too far south in the model, it is narrower than observed, and at a fixed latitude, while it tends to extend northwestward in the observations. The precipitation over the ice sheets, which was very excessive in model II, appears to be somewhat deficient with the present model. This large change may be due to use of the quadratic upstream finite differencing scheme, which maintains very strong gradients.

The planetary radiation balance is shown in Fig. 8. We show the model-data differences to emphasize the model shortcomings. Over low latitude ocean the planet is too bright in reflected sunlight by typically 20-30 W/m^2, and it is too dark over the oceans in the summer hemisphere. The discrepancy in outgoing longwave radiation is such as to reduce the discrepancy in the net incoming radiation. However, a substantial discrepancy remains in the summer hemisphere. This discrepancy is large enough to have important implications for the implied meridional heat transports, and thus for the drive of both atmosphere and ocean circulations. The cause of this discrepancy will be a focus of our model development experiments.

Overall, the model-data comparisons show that, despite some substantial errors, the simulated planet strongly resembles the Earth. This suggests that the model may be a useful guinea pig for experiments aimed at understanding how the Earth responds to different radiative perturbations. Thus the SI94 model is being used as the basis for several control runs and experiments with different climate forcings. At the same time, work aimed at improving the realism of the model is continuing, with the objective that future models should significantly reduce the deficiencies identified in the SI94 model.

Climate Variability

Observed year-to-year climate variability is a combination of changes arising from forcings, such as volcanic aerosols and greenhouse gases, and unforced fluctuations of the climate system. We wish to use the model to help determine how much of observed climate variability is forced and how much is unforced. The ability to do this depends in part on the realism of the unforced variability in the model, which is difficult to assess because observations necessarily contain both the forced and unforced components. However, we can get some indication of the model capability from the geographical and seasonal changes of variability, and also by examining how well the total variability approaches observations as the effects of known forcings are added to the model.

Here we examine the interannual variability of tropospheric temperature, for which consistent continuous observations are available from satellite MSU observations (Spencer et al., 1991). The top row of Fig. 9 shows the interannual standard deviation of tropospheric temperature for JJA and DJF for the 15 year period 1979-93 as measured by MSU channel 2. The second row shows the interannual variability of vertically weighted (Table 1) tropospheric temperature in run 1a of model SI94, that is in the absence of any climate forcings, the incoming solar irradiance and the lower boundary conditions of sea surface temperature and sea ice cover being identical year after year.

Apparently a large fraction of the variability at middle and high latitudes, especially in the winter hemisphere, is inherent in the unforced atmospheric variability. At low latitudes, on the other hand, the observed variability is considerably higher than that arising from the

atmosphere alone, a reflection of the large role of the El Nino/Southern Oscillation phenomena in low latitude climate.

The third and fourth rows in Fig. 9 show the tropospheric temperature variability in the model when year-to-year changes of atmospheric lower boundary conditions, specifically sea surface temperature (SST) and sea ice cover, are included in the simulations. The SST and sea ice variations are those used in the AMIP project (Gates, 1992) based on the data set of Reynolds and Marsico (1993). However, as shown in Section 6 below, the interannual sea ice variations are an order of magnitude larger than those in the real world.

Apparently the combination of unforced atmospheric variability and sea surface temperature variability provides a fairly realistic representation of observed variability. Of course the specified ocean variability partially includes the influence of climate forcings such as Pinatubo aerosols. When radiative forcings such as aerosol and ozone changes are added explicitly to the model, with the surface boundary conditions still specified, we anticipate only a small additional change in the simulated variability, mainly over continental regions.

Overall, the above results emphasize that a large portion of the interannual climate variability over the 15 year time frame is probably independent of forcings and is thus unpredictable. Furthermore, the additional variability associated with the specified interannual changes of the lower boundary conditions (SST and sea ice) must be only in part deterministic, and in part associated with unforced ocean variability. Of course even unforced ocean variability, although unpredictable on long time scales, has practical predictive value on short time scales because of the ocean's inertia. One objective of the full set of experiments we have outlined in our strategy of investigation (Section 3) is to help separate observed climate variability into components associated with different measurable forcings and different sources of unforced variability of the climate system.

The implication that most of the variability in the period 1979-93 is unforced, i.e., is a product of chaotic atmospheric dynamics, does not necessarily imply that we will not be able to identify a significant signal due to Pinatubo. As the different sources of variability add in a

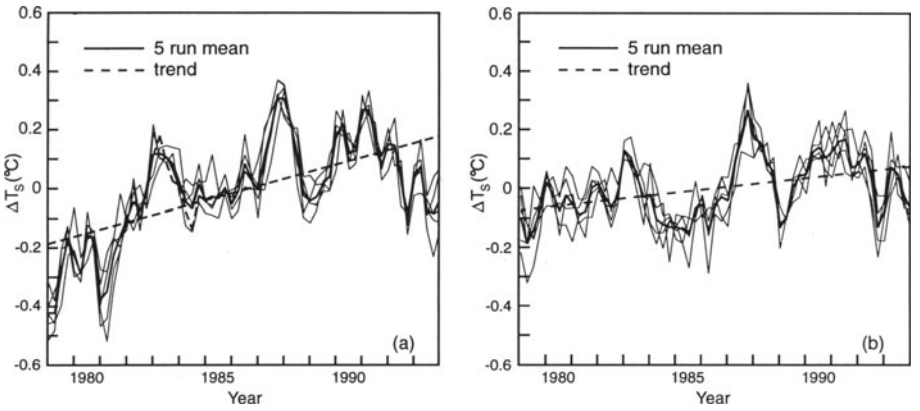

Figure 10. Global mean surface air temperature in (a) five simulations with AMIP time varying SST and sea ice (run 3 of GISS SI94 model), and (b) five simulations with time varying AMIP SST but with no interannual variability of sea ice (run 2). The mean trend in (a) is 0.24°C/decade, and in (b) it is 0.10°C/decade.

root-mean-square sense, a cooling over the period 1991-3 would not greatly alter the standard deviation for the full 15 year period.

Transient AMIP Simulations

The transient climate simulations with the AMIP SST and sea ice boundary conditions (run 3) were intended to be the basis for our analysis of climate change during the period 1979-present. However, calculation of the resulting trend of global surface air temperature in run 3 immediately raises a question about the realism of the AMIP boundary conditions. As shown in Fig. 10 the mean trend of global temperature in the five runs with AMIP boundary conditions is 0.24°C/decade, or 0.36°C over 1979-1993. This is much greater than the observed global temperature change, which is only about 0.1°C/decade (Hansen et al., 1995).

We have found that the principal cause of the large temperature trend in run 3 is the specified sea ice change in the AMIP boundary conditions (Fig. 11). This is the sea ice distribution used in the "blended" ship and satellite sea surface temperature analyses of Reynolds (1988) and Reynolds and Marsico (1993). It obviously involves a concatenation of three different

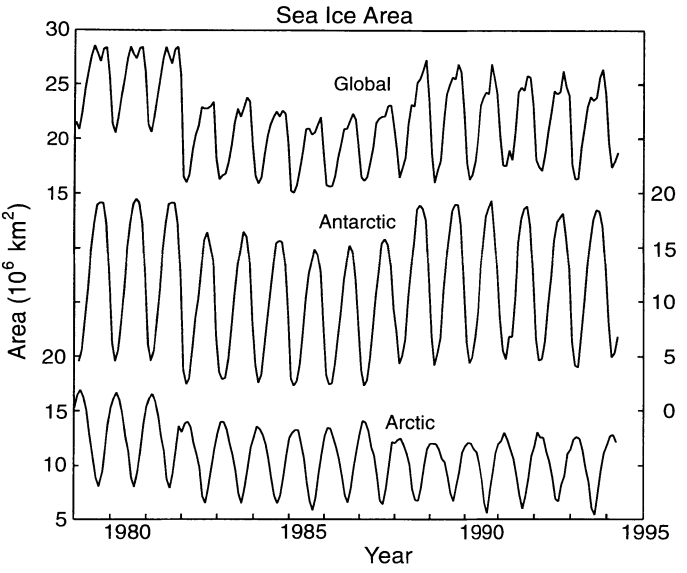

Figure 11. AMIP global sea ice cover used in run 3. The period 1982-87 was used to define a mean annual cycle of sea ice cover which was used for run 2.

sea ice data sets, with discontinuities at the end of 1981 and the end of 1987. The jumps in sea ice cover at those times are an order of magnitude larger than any interannual changes of sea ice cover in homogeneous sea ice data sets derived from satellite microwave observations (Gloersen et al., 1992; Figs. 5.2.1 and 5.2.3).

As a verification of the impact of the sea ice changes on global temperature, we used the sea ice cover from a period with a homogeneous analysis, 1982-87, to define a mean annual cycle of sea ice. The average sea ice area during that interval is about 20 million square kilometers, close to the value in the satellite microwave data (Gloersen et al., 1992). The 1982-87 mean (seasonally varying) sea ice distribution was combined with the interannually varying SSTs of Reynolds and Marsico (1993) and used as the lower boundary condition for control run 2. The resulting global temperatures (Fig. 10b) yielded a more realistic trend of 0.10°C/decade over the period 1979-93.

We conclude that the AMIP ocean boundary conditions are not satisfactory for analysis of climate change during the period 1979-present. A considerable improvement is obtained by simply replacing the variable sea ice by an unchanging mean annual cycle. However, it is obviously desirable to put together a combined SST and sea ice data set which incorporates the high precision satellite microwave measurements of sea ice concentration.

Pinatubo Radiative Forcing

A prerequisite to use of Pinatubo as a test of the climate system's response to a radiative forcing is accurate definition of the Pinatubo aerosol climate forcing. The aerosol properties employed by Hansen et al. (1992) in their climate model predictions were only a crude estimate, with the optical depth guessed on the basis of a few early data points and the aerosol size distribution assumed to be similar to that measured at one location after the earlier volcano El Chichon.

Now it is possible to extract much more accurate data on Pinatubo aerosol optical depths and particle sizes from available measurements. Also, Earth Radiation Budget Experiment (ERBE) satellite measurements of flux anomalies at the top of the atmosphere provide a fundamental check on the computed forcing. Of course ERBE flux anomalies are influenced by any other changes that may have occurred in radiative constituents and by unforced climate fluctuations in the period after the eruption. But the Pinatubo aerosol forcing is sufficiently large that it is reasonable to expect it to dominate the global radiative flux anomalies for a year or so after the eruption.

We first compare the radiation balance anomalies observed by ERBE (Minnis et al., 1993) with the same quantities calculated in the climate simulations of Hansen et al. (1992), hereafter referred to as the GRL92 model. As the observations cover only the region from 40°N to 40°S, we compare the model and data for that limited region in Fig. 12. It is apparent that the net forcing at these latitudes is substantially larger in the model than in the ERBE observations. Integrated from June 1991 to the end of 1992 the calculated net radiation anomaly was -4.1 W years/m^2 compared to an observed anomaly of -2.1 W years/m^2. Part of this discrepancy is accounted for by the fact that, as mentioned by Hansen et al. (1992),

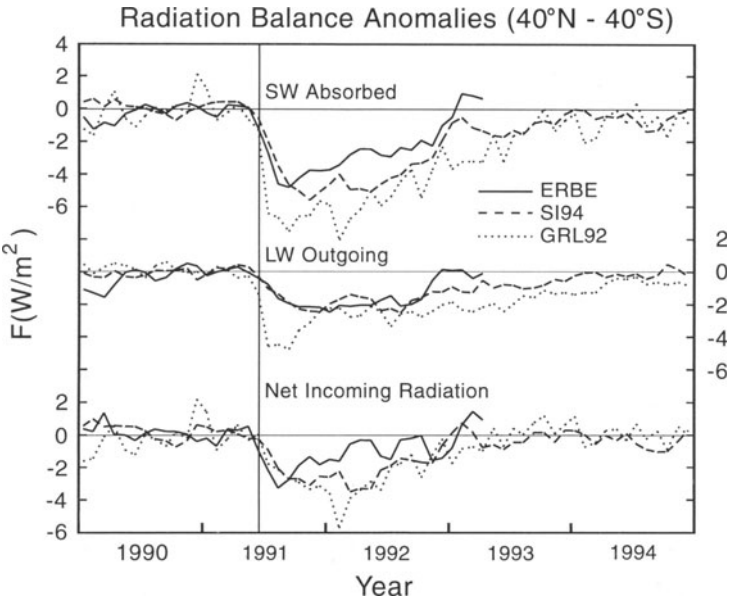

Figure 12. Radiation balance anomalies observed by ERBE for latitudes 40°S-40°N (Minnis et al., 1993), with the mean for the period 1985-89 used to remove the seasonal cycle and with the zero point defined by the mean anomaly for the 12 months preceding the month of the Pinatubo eruption. Model radiation balance anomalies are from the simulations of Hansen et al. (1992) and from our current simulations with the SI94 climate model and the SI94 aerosols.

the radiative parameterization in the GRL92 GCM overstated aerosol forcings at low latitudes by about 10% while understating the forcings at high latitudes by a comparable amount. With the more accurate radiative parameterization in the SI94 model and with the more realistic SI94 aerosols, defined below, the integrated net radiation anomaly is -3.4 W years/m^2. Further improvements in knowledge of the aerosol properties seem unlikely to alter this calculated forcing much. The uncertainty in the measured ERBE forcing has not been established; refinements in the ERBE data processing are presently being implemented. As shown in Fig. 12, the difference of just over 1 W year/m^2 occurs in the absorbed shortwave radiation. If this difference can be shown to be meaningful, it would affect interpretation of the climate sensitivity to volcanic aerosol forcing, as it reduces the forcing by more than one-third. Note that the cloud alteration required to account for this difference is a decrease of cloud albedo

after the Pinatubo eruption, opposite in sense to the aerosol impacts on clouds which are usually hypothesized.

Our primary source of Pinatubo aerosol information is the SAGE II data (McCormick et al., 1995). SAGE II measured the optical thickness of the aerosols at four wavelengths between 0.385 and 1.02 μm, although frequent saturation of the signal during the first several months after the eruption required extrapolation to estimate the optical depth to the tropopause. One of us (AL) used the multispectral SAGE II optical depth data to estimate at each latitude and month the aerosol effective radius providing best least-mean-square fit at the four wavelengths for several assumed values of the effective variance of a monomodal (gamma) size distribution (Hansen and Travis, 1974). Comparison of the resulting optical depths at 12.1 μm with ISAMS data (Lambert et al., 1993) indicates that a fixed effective variance of 0.35 provides reasonable agreement with both ISAMS data (Fig. 14) and SAGE II data. Although the actual size distribution may be bimodal or trimodal (P. Russell et al., 1995) and vary substantially with altitude, the result we have inferred may be a good approximation for the climate forcing because it has been tied down to match observed optical depths at a broad range of wavelengths from the ultraviolet to 12 μm.

Detailed results from the particle size distribution analysis will be presented elsewhere. The effective radius (Fig. 13b) was found to increase with time [unlike the assumed particle sizes in the GRL92 simulation], reaching a (global average) maximum of about 0.56 in October 1992, 16 months after the eruption. The inferred global mean effective radius was 0.5 μm or larger from January 1992 through April 1993. Such a growth of Pinatubo aerosols with time was previously deduced from Mauna Loa optical depth spectra (Russell et al., 1993). We calculate the optical depth at 0.55 μm (Fig. 13a) from our inferred size distribution and the measured optical depth at 1.02 μm. Apparently the optical depth assumed by Hansen et al. (1992) was remarkably prescient (Fig. 13a).

However, the accurate guess of the aerosol optical depth at visible wavelengths by Hansen et al. (1992) does not mean that their aerosol climate forcing was accurate. The net radiative forcing depends on the optical depths at other wavelengths, especially in the thermal infrared region which determines the greenhouse effect of the aerosols. Fig. 14 illustrates how the

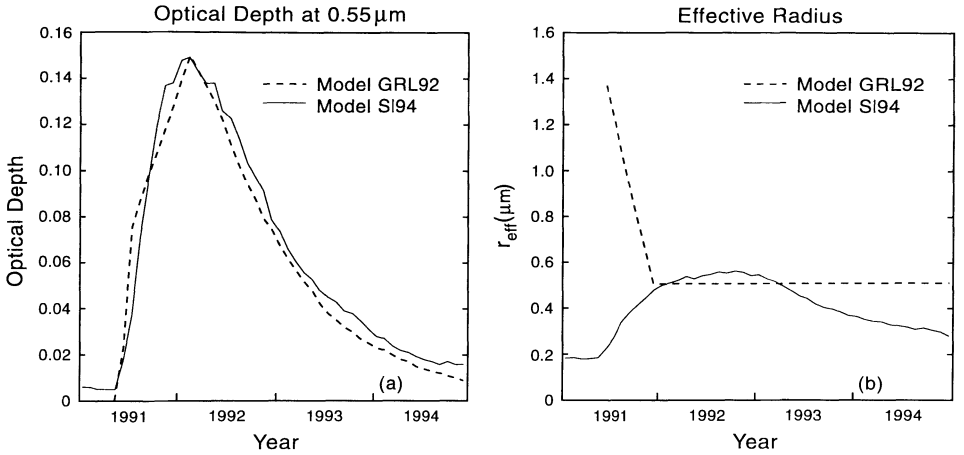

Figure 13. Global mean aerosol (a) optical depth at 0.55 μm and (b) effective particle radius as assumed in the GRL92 model (Hansen et al., 1992) and as being used in the SI94 model. The optical depth and effective radius in the SI94 model, which vary with time and latitude, were derived from multispectral SAGE observations assuming a monomodal size distribution with effective variance 0.35, the latter based on the constraint of fitting ISAMS observations at 12.1 μm.

inferred optical depth varies as a function of the assumed effective variance of the size distribution, v_{eff}. Based on the measured ISAMS optical depths at 12.1 μm, we choose the results for the size distribution with v_{eff} = 0.35 as the approximation we will use for our climate simulations with the SI94 model. In reality v_{eff} must vary with time. With the bimodal size distribution used in GRL92, v_{eff} decreased linearly from 0.41 in June 1991 to 0.15 in December 1991, after which it remained 0.15. We believe that it is a much better approximation to take v_{eff} = 0.35 during the time of substantial aerosol optical depth, but further investigation of the size distribution is worthwhile.

This relatively broad size distribution yields a somewhat greater greenhouse effect than the size distribution used by Hansen et al. (1992) and a somewhat smaller solar forcing, both as illustrated in Fig. 15. As a result the maximum net forcing in the SI94 model is about 3.5 W/m^2, which compares to about 4 W/m^2 for the aerosol properties assumed by Hansen et al. (1992), when evaluated with the same accurate radiation program. In addition, as mentioned

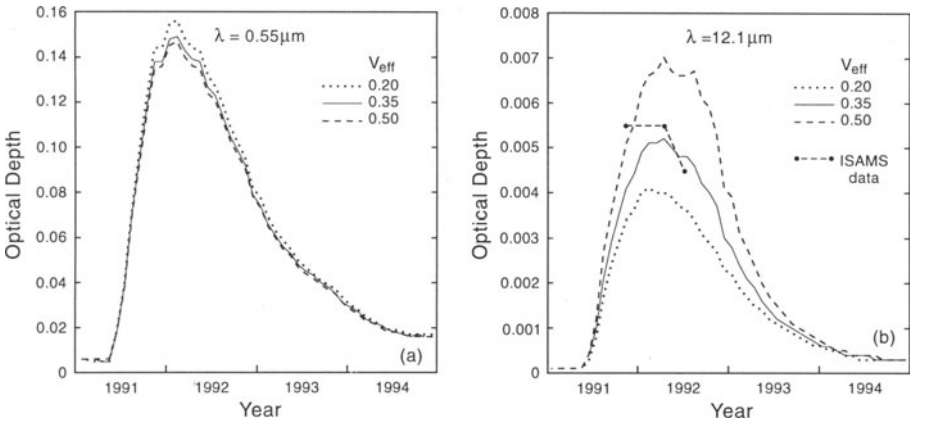

Figure 14. Global mean aerosol optical depth at 0.55 and 12.1 μm for several values of effective variance, v_{eff}. ISAMS observations at 12.1 μm are reported by Lambert et al. (1993). The effective radius varies with time and latitude so as to provide optimum fit to the multispectral optical depths measured by SAGE II.

above, the multiple scattering approximations in the GCM of Hansen et al. (1992) exaggerated the forcing at low latitudes by about 10% and understated the forcing at high latitudes.

The SI94 aerosols described here are presently being used to drive climate simulations with the SI94 climate model. We believe that the SI94 aerosol properties are much more realistic than the GRL92 aerosol properties. However, we are continuing to investigate additional sources of aerosol information and plan to assess whether further refinements of the aerosol properties are warranted.

Discussion

Extraction of the potential information about the Earth's climate system provided by a large volcanic eruption requires both accurate global observations and a broad strategy for modeling and analysis. We have outlined here our plan for investigation of the Pinatubo eruption and described some initial difficulties in its implementation.

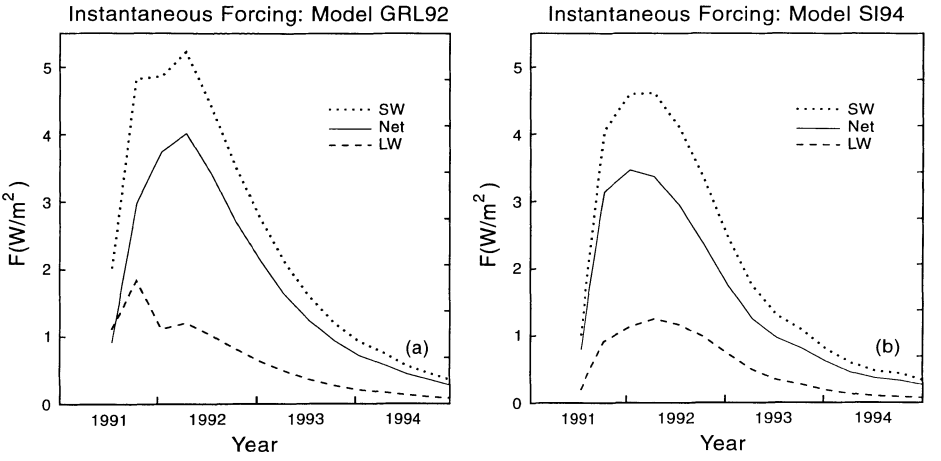

Figure 15. Seasonally averaged instantaneous radiative forcings for the aerosol properties (a) assumed in the GRL92 model, and (b) to be used in the SI94 model. The forcings for both cases were computed with the radiative transfer program of the SI94 model.

We find that the maximum of the mean cooling following the five greatest eruptions of the past century is only about 0.25°C, but there is evidence of a cooling effect continuing for up to 5-7 years. As the ocean plays a key role in determining the magnitude and time scale of the climate response, our investigation of Pinatubo will employ several different ways of simulating the ocean.

We have identified major shortcomings in the first atmospheric model being employed for our Pinatubo simulations, SI94. At the same time that we carry out simulations with SI94 we are developing an improved version of the model, which will be used to help us assess how sensitive our interpretations are to model limitations.

We have used our atmospheric model with specified climatological surface boundary conditions to illustrate that unforced atmospheric variability, i.e., unpredictable chaotic fluctuation, accounts for a large fraction of interannual surface climate variability during the 15 year period 1979-93, especially in the winter hemisphere. This does not imply that we will be unable to discern regional climate effects of Pinatubo, but calculated regional effects will

need to be couched in probabilistic terms, and it may be difficult to identify with confidence Pinatubo climate impacts in the winter.

We have found that the AMIP surface boundary conditions are unsuitable for studies of interannual global climate change. Specifically, the AMIP sea ice cover has some unrealistic discontinuities. There are available satellite microwave sea ice observations which could be used to provide much more realistic surface boundary conditions.

We have found that multispectral satellite measurements provide strong constraints on the stratospheric aerosol size distribution after Pinatubo, and thus that it should be possible to accurately define the climate forcing due to the Pinatubo aerosols. We calculate that the peak forcing occurred in early 1992 and was about 3.5 W/m^2. This aerosol forcing is now being used in simulations with the SI94 model.

Acknowledgements. We thank Howard Gordon for suggesting ocean albedo parameterizations accounting for foam at high wind speed and subsurface scattering, Christina Koizumi for desktop publishing, Elaine Matthews for providing improved land surface specifications, and Richard Stothers for information on historical volcanic eruptions.

References

Abramopoulos F (1991) A new fourth-order enstrophy and energy conserving scheme, Mon Wea Rev 119: 128-133

AGU (1992) Volcanism and Climate Change, American Geophysical Union Special Report ISBN 87590-818-7, Washington, 27 pp

Barkstrom B, Harrison E, Smith G, Green, R Kibler J, Cess R (1989) Earth Radiation Budget Experiment (ERBE) Archival and April 1985 Results, Bull Amer Meteorol Soc 70: 1254-1262

Del Genio AD, Yao MS (1993) Efficient cumulus parameterization for long-term climate studies: the GISS scheme, Amer Meteorol Soc Mono 46: 181-184

Del Genio AD, Yao MS, Kovari W, Lo KKW (1995) A prognostic cloud water parameterization for global climate models, J Climate (submitted)

Dutton EG, Christy JR (1992) Solar radiative forcing at selected locations and evidence for global lower tropospheric cooling following the eruptions of El Chichon and Pinatubo, Geophys Res Lett 19: 2313-2316

Forsyth PY (1988) In the wake of Etna, 44 BC, Classical Antiquity 7: 49-57

Franklin B (1784) Meteorological imaginations and conjectures Paper read December 22, 1784 to Literary and Philosphical Society of Manchester, reprinted by Sigurdsson (1982)

Gates WL (1992) AMIP: the atmospheric model intercomparison project, Bull Amer Meteorol Soc 73: 1962-1970

Gelman ME (1991) Stratospheric monitoring with TOVS data, Palaeogeo Palaeoclim Palaeoecol 90: 75-78

Gilliland RL, Schneider SH (1984) Volcanic, CO2 and solar forcing of Northern and Southern Hemisphere surface air temperatures, Nature 310: 38-41

Gloersen P, Campbell WJ, Cavalieri DJ, Comiso JC, Parkinson CL, Zwally HJ (1992) Arctic and Antarctic Sea Ice, 1978-1987, NASA SP-511, Washington DC, 290 pp

Graf HF, Kirchner I, Robock A, Schult I (1993) Pinatubo eruption winter climate effects: model versus observations, Clim Dyn 9: 81-93

Graf HF, Perlwitz J, Kirchner I (1994) Northern Hemisphere tropospheric mid-latitude circulation after violent volcanic eruptions, Beitr Phys Atmosph 67: 3-13

Handler P (1986) Possible association between the climatic effects of stratospheric ae 0 '37nd sea surface temperatures in the eastern tropical Pacific Ocean, J Climatology 6: 31-41

Hansen J, Fung I, Lacis A, Rind D, Lebedeff S, Ruedy R, Russell G, Stone P (1988) Global climate changes as forecast by Goddard Institute for Space Studies three-dimensional model, J Geophys Res 93: 9341-9364

Hansen J, Lacis A, Rind D, Russell G, Stone P, Fung I, Ruedy R, Lerner J (1984) Climate sensitivity: analysis of feedback mechanisms, Geophys Mono 29: 130-163

Hansen J, Lacis A, Ruedy R, Sato M (1992) Potential climate impact of Mount Pinatubo eruption, Geophys Res Lett 19: 215-218

Hansen J, Lacis A, Ruedy R, Sato M, Wilson H (1993) How sensitive is the world's climate? Res Explor 9:142-158

Hansen JE, Lebedeff S (1987) Global trends of measured surface air temperature, J Geophys Res 92: 13345-13372

Hansen J, Russell G, Rind D, Stone P, Lacis A, Lebedeff S, Ruedy R, Travis L (1983) Efficient three-dimensional global models for climate studies: models I and II, Mon Wea Rev 111: 609-662

Hansen JE, Travis LD (1974) Light scattering in planetary atmospheres, Space Sci Rev 16: 527-610

Hansen JE, Wang WC, Lacis AA (1978) Mount Agung eruption provides test of a global climatic perturbation, Science 199: 1065-1068

Hansen J, Wilson H, Sato M, Ruedy R, Shah K, Hansen E (1995) Satellite and surface temperature data at odds? Climatic Change (in press)

Harrington CR (1992) The Year Without a Summer Canadian Museum of Nature, Ottawa, 576 pp

Hartke GJ, Rind D (1995) An improved boundary layer model for the GISS GCM (in preparation)

Hofmann DF, Rosen JM (1983) Sulfuric acid droplet formation and growth in the stratosphere after the 1982 eruption of El Chichon, Science 222: 325-327

Hunt BG (1977) A simulation of the possible consequences of a volcanic eruption on the general circulation of the atmosphere, Mon Wea Rev 105: 247-260

Intergovernmental Panel on Climate Change (1992) Climate Change 1992, The Supplementary Report to the IPCC Scientific Assessment Houghton JT, Callander BA, Varney SK (eds), Cambridge Univ Press, 200 pp

Jensen EG, Toon OB (1992) The potential effects of volcanic aerosols on cirrus cloud microphysics, Geophys Res Lett 19: 1759-1762

Jiang X, Fung I (1994) Ocean response to surface heat anomalies, J Climate, 7: 783-791

Kodera K (1993) Influence of the stratospheric circulation change on the troposphere in the Northern Hemisphere winter, in The Role of the Stratosphere in Global Change, ML Chanin ed, Springer-Verlag, Berlin, pp 227-243

Kodera K, Yamazaki K (1994) A possible influence of recent polar stratospheric coolings on the troposphere in the northern hemisphere winter, Geophys Res Lett 21: 809-812

Lambert A, Grainger RG, Remedios JJ, Rodgers CD, Corney M, Taylor FW (1993) Measurements of the evolution of the Mt Pinatubo aerosol cloud by ISAMS, Geophys Res Lett 20: 1287-1290

Legates DR, Willmott CJ (1990a) Mean seasonal and spatial variability in global surface air temperature, Theor Appl Climatol 41: 11-21

Legates DR, Willmott CJ (1990b) Mean seasonal and spatial variability in gauge-corrected, global precipitation, Inter J Climatol 10: 111-127

MacCracken MC, Luther FM (1984) Preliminary estimate of the radiative and climatic effects of the El Chichon eruption, Geofisica Internacional 23: 385-401

Marengo J, Druyan L (1994) Validation of model improvements for the GISS GCM, Clim Dyn 10: 163-179

Mass C, Schneider SH (1978) Statistical evidence on the influence of sunspots and volcanic dust on long-term temperature trends, J Atmos Sci 34, 1995-2004

Matthews E (1983) Global vegetation and land-use: new high-resolution data bases for climate studies, J Clim Appl Meteorol 22: 474-487

Matthews E, (1984) Prescription of land-surface boundary conditions in GISS GCM II: a simple method based on fine-resolution data bases, NASA Technical Memorandum 86096

McCormick MP, Thomason LW, Trepte CR (1995) Atmospheric effects of the Mt Pinatubo eruption, Nature 373: 399-404

Miller RL, Jiang X (1995) Surface heat fluxes and coupled variability in the tropics of a coupled general circulation model, J Climate (in press)

Minnis P, Harrison EF Stowe LL, Gibson GG, Denn FM, Doelling DR, Smith WL (1993) Radiative climate forcing by the Mount Pinatubo eruption, Science 259: 1411-1415

Mitchell JM (1961) Recent secular changes of global temperature, Ann N Y Acad Sci 95, 235-250

NOAA (1995) Sixth Annual Climate Assessment 1994 NOAA Climate Analysis Center, Camp Springs Md (in press)

Oort AH (1983) Global Atmospheric Circulation Statistics, 1958-1973, NOAA Prof Paper 14, Rockville Md, 180 pp

Prather MJ (1986) Numerical advection by conservation of second order moments, J Geophys Res 91: 6671-6680

Reynolds RW (1988) A real-time global sea-surface temperature analysis, J Climate 1: 75-86

Reynolds RW, Marsico DC (1993) An improved real-time global sea surface temperature analysis, J Climate 6: 114-119

Rind D, Balachandran NK, Suozzo R (1992) Climate change and the middle atmosphere part II: the impact of volcanic aerosols, J Climate 5: 189-208

Rind D, Suozzo R, Balachandran NK, Lacis A, Russell G (1988) The GISS global climate/middle atmosphere model Part I: model structure and climatology, J Atmos Sci 45: 371-386

Robock A (1983) The dust cloud of the century, Nature 301: 373-374

Robock A (1984) Climate model simulations of the effects of the El Chichon eruption, Geof Int 23: 403-414

Robock A (1991) The volcanic contribution to climate change of the past 100 years, in Greenhouse-Gas-Induced Climatic Change: A Critical Evaluation of Simulations and Observations, ed ME Schlesinger, Elsevier, Amsterdam, pp 429-443

Robock A, Mao J (1992) Winter warming from large volcanic eruptions, Geophys Res Lett 12: 2405-2408

Rosenzweig C, Abramopoulos F (1995) Land surface model development for the GISS GCM, J Climate (submitted)

Rossow WB, Zhang YC (1995) Calculation of the top-of-the-atmosphere radiative fluxes from physical quantities derived from ISCCP data sets Part II: validation and results, J Geophys Res 100: 1167-1197

Russell GL, Miller JR, Rind D (1995) A coupled atmosphere-ocean model for transient climate change studies, Atmos Ocean (submitted)

Russell PB, Livingston JM, Dutton EG, Pueschel RF, Reagan JA, DeFoor TE, Box MA, Allen D, Pilewskie P, Herman BM, Kinne SA, Hofmann DJ (1993) Pinatubo and pre-Pinatubo optical depth spectra: Mauna Loa measurements, comparisons, inferred particle size distributions, radiative effects, and relationship to lidar data, J Geophys Res 98: 22,969-22,985

Russell PB, Livingston JM, Pueschel RF, Pollack JB, Brooks SL, Hamill PJ, Hughes JJ, Thomason LW, Stowe LL, Deshler T, Dutton EG, Bergstrom RW (1995) Global to microscale evolution of the Pinatubo volcanic aerosol, derived from diverse measurements and analyses, J Geophys Res (submitted)

Sassen K, Starr DO, Mace GG, Poellot MR, Melfi SH, Eberhard WL, Spinhirne JD, Elorante EW, Hagen DE, Hallett J (1995) The 5-6 December 1991 FIRE II jet stream cirrus case study: possible influences of volcanic aerosols, J Atmos Sci 52: 97-132

Sato M, Hansen JE, McCormick MP, Pollack JB (1993) Stratospheric aerosol optical depths, 1850-1990, J Geophys Res 98: 22,987-22,994

Schneider SH, Mass C (1975) Volcanic dust, sunspots, and temperature trends, Science 190: 741-746

Self S, Rampino MR (1988) The relationship between volcanic eruptions and climate change: still a conundrum? Eos 69: 74-86

Shah KP, Rind D (1995) Use of microwave brightness temperatures with a general circulation model, J Geophys Res (in press)

Sigurdsson H (1982) Volcanic pollution and climate: the 1783 Laki eruption, EOS Trans Amer Geophys Union 63: 601-603

Spencer RW, Christy JR (1993) Precision lower stratospheric temperature monitoring with the MSU: technique, validation, and results 1979-1991, J Clim 6: 1194-1204

Spencer RW, Christy JR, Grody NC (1991) Precision tropospheric temperature monitoring 1979-90, Palaeogeog Palaeoclim Palaeoecol 90: 113-120

Stommel H, Stommel E (1979) The year without a summer, Sci Amer 240 176-186

Stommel H, Stommel E (1983) Volcano Weather, the Story of 1816, The Year Without a Summer, Seven Seas Press, Newport, RI, 177 pp

Stothers RB (1984) The great Tambora eruption in 1815 and its aftermath, Science 224: 1191-1198

Stothers RB, Rampino MR (1983) Volcanic eruptions in the Mediterranean before AD 630 from written and archaeological sources, Geophy Res 88 6357-6371

Wang PH, Minnis P, Yue GK (1995) Extinction coefficient (1 um) properties of high-altitude clouds from solar occultation measurements (1985-1990): evidence of volcanic aerosol effect, J Geophys Res 100: 3181-3199

Wilson C (1992) Workshop on World Climate in 1816: a summary and discussion of results in The Year Without a Summer? World Climate in 1816, ed CR Harrington, Canadian Museum of Nature, Ottawa, pp 523-555